Journal of Modern Optics
Publication details, including instructions for authors and subscription information:
http://www.tandfonline.com/loi/tmop20

Two center and Coulomb effects in near-threshold ionization of H^+_2 by short laser pulses

M.F. Ciappina [a] & W.R. Cravero [b]

[a] Max Planck Institute for the Physics of Complex Systems, Dresden, Germany

[b] CONICET and Departamento de Física, Universidad Nacional del Sur, Bahía Blanca, Argentina

Version of record first published: 27 Jul 2010.

To cite this article: M.F. Ciappina & W.R. Cravero (2009): Two center and Coulomb effects in near-threshold ionization of H^+_2 by short laser pulses, Journal of Modern Optics, 56:1, 11-26

To link to this article: http://dx.doi.org/10.1080/09500340802409900

Journal of Modern Optics
Vol. 56, No. 1, 10 January 2009, 11–26

Taylor & Francis
Taylor & Francis Group

Two center and Coulomb effects in near-threshold ionization of H_2^+ by short laser pulses

M.F. Ciappina[a]* and W.R. Cravero[b]

[a]*Max Planck Institute for the Physics of Complex Systems, Dresden, Germany;* [b]*CONICET and Departamento de Física, Universidad Nacional del Sur, Bahía Blanca, Argentina*

(*Received 24 July 2008; final version received 14 August 2008*)

We investigate the influence of the Coulomb potential as well as the two center contribution in the angle-resolved photoelectron spectrum, resulting from the single ionization of H_2^+ molecules by short laser pulses. We present an extension of the Coulomb–Volkov distorted wave approximation to the H_2^+ case. This last model can be considered as an improvement beyond the strong-field approximation (SFA) and was capable of reproducing the structures present in near-threshold ionization in atoms.

Keywords: molecules; strong-field ionization; above-threshold ionization; Coulomb–Volkov model

1. Introduction

Processes involving molecular species are sensitive to their structure and composition. In particular, the presence of two or more atomic sites have led to the observation of quantum mechanical interference effects. Within the laser–matter area, high-order harmonic generation (HHG) in H_2^+ and H_2 have shown to be a particular scenario for observing and studying these interference effects on a sub-Ångstrom spatial scale (see [1] for a comprehensive review).

Other related atomic processes, in which interference patterns appear, are single ionization of simple molecules, e.g. H_2^+ and H_2, by photon [2,3], electron [4,5] or ion impact [6,7]. For such processes, there is a persisting effort to model the initial (bound) and final (continuum) electronic channels. In many cases, the molecular ground state is well approximated using a linear combination of atomic orbitals (LCAO). On the other hand, the continuum electron in the presence of two atomic centers is quite difficult to model, given the lack of an exact solution of the Schrödinger equation for three or more particles with Coulomb interactions. Nevertheless, a large number of approximated models have been able to reproduce the available experimental data reasonably well. For electron impact ionization of H_2^+ and H_2 several approaches have been used that take into account the multicenter nature of the initial and final molecular wave functions. These theories have been used to predict experimental results with reasonable success [8–10]. Additionally, it was found that, using two center electronic wave functions in the recombination step in the HHG calculation in H_2^+, the prediction of the interference minima are comparable to that resulting from the numerical solution of the time-dependent Schrödinger equation (TDSE) [11].

Focusing within the area of intense laser–molecule interactions, interference patterns appear in several processes such as the above cited high order harmonic generation (HHG) and above-threshold ionization (ATI) [12–19]. Due to the two-center interference effect, the harmonic spectrum in diatomic molecules exhibits a strong dependence on the molecular orientation so that the suppression or enhancement of certain harmonic-frequency ranges is possible (see e.g. [1] and references therein).

The theoretical approaches to deal with HHG and ATI in atoms can be divided in two broad groups: (i) *ab initio* solutions of the TDSE in one or more dimensions [20,21], and (ii) quantum mechanical approximated methods based on a more phenomenological approach, e.g. the SFA [22–28]. In molecules, the solution of the TDSE represents a big computational challenge, and only spatial-reduced schemes have been applied so far (see e.g. [1]). As a consequence of this, the development and utilization of approximated models to predict laser-induced molecule processes are very much welcomed.

The advent of COLTRIMS experiments has provided the theoreticians with the possibility of performing stringent tests on the different theoretical approaches, since the *imaging* of the vectorial momentum distribution of the reaction fragments is easily achievable. A recent set of experiments have shown a complex emission pattern in the two-dimensional

*Corresponding author. Email: ciappinam@ihpc.a-star.edu.sg
Present address: Institute of High Performance Computing, Singapore

ISSN 0950–0340 print/ISSN 1362–3044 online

DOI: 10.1080/09500340802409900
http://www.informaworld.com

momentum plane, parallel and perpendicular to the laser polarization axis, of the laser-ionized electron distributions near threshold, using rare-gas atoms [29,30]. Theoretical analysis revealed that these diffraction oscillations are a result of the interference of classical paths of the electron, released at different times, but reaching the same Kepler asymptote in a classical description of the electron kinematics in a Coulomb field [31].

In order to provide another test for laser-induced ionization theories, analysis of the momentum distribution transverse to the polarization axis have been performed. It has been shown that, to leading order, the (nonrelativistic) electric field of the laser does not transfer momentum in this direction. In accordance with the first experiments reported in [32,33], a smooth Gaussian transverse distribution was predicted by the seminal tunneling theory of Delone and Krainov (DK), in which Coulomb interactions are treated as a weak perturbation [22]. Methods based on the SFA approach also exhibits a Gaussian-like transverse momentum distribution [22,34,35]. Contrarily to these predictions, recently high-resolution experiments for single ionization of rare-gas atoms [36] showed spectra exhibiting a sharp cusp-like structure around zero transverse momentum. Simulations using a Classical Trajectory Monte Carlo (CTMC)-based approach, including tunneling, reproduce the cusp shape when the Coulomb interaction of the laser-ionized electron with the residual parent ion is taken into account. On the other hand, when the Coulomb interaction is neglected after tunneling, a Gaussian distribution is recovered in accordance with the DK theory [34,35]. Summarizing, calculations based on the SFA in atoms fail to properly reproduce both the correct shape pattern near the threshold in the doubly-differential momentum distribution and the cusp at origin in the transversal momentum distribution. The inclusion of Coulomb-residual effects into the final state has been found to be important for total laser-induced ionization rates [37] and in the description of the *bouquet-type* structures and in the right–left (also called forward–backward) asymmetry of photoelectron spectra produced by short laser pulses in atoms (see e.g. [35] and references therein).

Regarding laser-induced molecular processes, Yudin et al. [38], have shown the importance of the Coulomb continuum effects in the production of asymmetric molecular interference in photoionization, photorecombination, bremsstrahlung and Compton ionization in H_2^+ molecules. They employed Coulomb–Volkov wavefunctions to model the interaction between the laser-ionized electron and the two ionic cores. In further studies, a theoretical description of x-ray photoionization of H_2^+ based on the sudden approximation using Coulomb–Volkov continuum electron wavefunctions, was presented [39]. Finally in [40] the authors have disentangled the different *zoo* of interference structures that appear in photoionization of H_2^+ molecules by intense laser pulses and have shown that the Coulomb–Volkov continuum wave functions are a powerful tool to extract the attosecond features arising in this laser-induced process.

In this work an extension of the Coulomb–Volkov distorted-wave approximation (CVA) to describe the complex near-threshold energy region of photoemission spectra in H_2^+ is presented. The CVA is considered as a time-dependent distorted-wave approach [24,25] and allows us to include the effect of the remaining ionic cores in the final state at the same level of approximation as the laser field. In this way, turning on and off the Coulomb interaction we can directly probe the effect of the core potential on the dynamics of the laser-detached electron. The CVA predictions are compared with values derived from the SFA, i.e. neglecting the Coulomb influence, and with those considering the incoherent contribution of the atomic sites, i.e. neglecting the two center nature of the molecule considering it as an atomic-like system. With this analysis we can clearly identify both the Coulomb contributions and the two center effects in the electron emission spectra. As in the case of atoms, we show that the inclusion of the Coulomb potential within the CVA leads to the appearance of near threshold *bouquet-shape* patterns in doubly-differential momentum distributions.

In the next section we describe the time-dependent distorted-wave theory extended to the molecular case. Also the well-known SFA or strong-field approximation will be pointed out, together with the differences between the CVA. In Section 3 we discuss results for the formation of the low-energy structures in the doubly-differential electron momentum distributions, together with an analysis of the contributions both of the Coulomb potential and the two center atomic sites. Atomic units (au) are used throughout this article unless otherwise indicated.

2. Theories

We consider the interaction of an H_2^+ molecule with a short laser pulse, which is described through a time-dependent electric field along the $\widehat{z}$ direction (linear polarization). The explicit expression for the field $\boldsymbol{E}(t)$ reads

$$\boldsymbol{E}(t) = f(t)\cos(\omega_0 t + \phi_{\mathrm{CE}})\widehat{z}, \tag{1}$$

where ω_0 is the laser frequency, ϕ_{CE} the relative carrier-envelope phase, and $f(t)$ is the so-called *envelope*

function of the pulse, $f(t) = E_0 \cos^2(\pi t/\tau)$ for $t \in [-\tau/2, \tau/2]$ and 0 otherwise, τ being the total duration of the pulse and E_0 the electric field strength. Due to the interaction with the laser field, the electron initially bounded to both H nuclei, is emitted to the continuum with momentum $\boldsymbol{k}$ and energy $\epsilon_f = k^2/2$. Upon the conclusion of the pulse, we consider the electron to be in an unperturbed final state $|\phi_f\rangle$. We describe the initial electronic state $|\phi_i\rangle$ as a LCAO, with an hydrogenic 1s state, centered in each nuclei of the molecule (see above).

The time evolution of the electronic state $|\psi(t)\rangle$ is governed by the TDSE with a Hamiltonian of the type $H(t) = H_0 + V_L(t)$ where H_0 is the time independent molecular Hamiltonian and $V_L(t) = \boldsymbol{r} \cdot \boldsymbol{E}(t)$ represents the interaction of the electron with the laser field, formulated in the length gauge.

We are interested in double-differential electron momentum distributions, that can be calculated from the transition matrix T_{if}, i.e. the T-matrix element corresponding to the transitions $|\phi_i\rangle \to |\phi_f\rangle$, as follows

$$\frac{dP}{d\boldsymbol{k}} = |T_{if}|^2. \tag{2}$$

The transition amplitude T_{if} can be computed using different approximations, as we will show next. Further, according to the internuclear separation mentioned in the last paragraph, it is possible to analyze the contribution of each H nucleus independently.

According to the time-dependent distorted wave theory [41], two different formulations may be used to calculate the transition amplitude T_{if}: the *post* and *prior* versions. Following [35] we employ the post version, that can be written formally as

$$T_{if} = -i\int_{-\infty}^{+\infty} dt \langle \chi_f^-(t)|V_L(t)|\phi_i(t)\rangle, \tag{3}$$

where $\chi_f^-(t)$ is the final *distorted-wave* function and $\phi_i(t)$ represent the electronic initial state satisfying

$$i\frac{\partial}{\partial t}|\phi_i(t)\rangle = H_0|\phi_i(t)\rangle = \left(\frac{p^2}{2} + V_C\right)|\phi_i(t)\rangle = \epsilon_i|\phi_i(t)\rangle, \tag{4}$$

where $V_C = V_1 + V_2$ represents the nuclei potential and $\epsilon_i = 1.1$ au (30 eV) the H_2^+ binding energy. For the initial electronic state we use an LCAO, i.e. the ground state H_2^+ molecular wave function is taken to be

$$\phi_i(\boldsymbol{r}, \boldsymbol{R}) = \frac{1}{(2[1 + s(R)])^{1/2}}[\psi_h(\boldsymbol{r}_1) + \psi_h(\boldsymbol{r}_2)], \tag{5}$$

with $\psi_h(\boldsymbol{r})$ being the ground state of the hydrogen atom, $\boldsymbol{r}_1 = \boldsymbol{r} + \boldsymbol{R}/2$ and $\boldsymbol{r}_2 = \boldsymbol{r} - \boldsymbol{R}/2$ denote the position of each H atom and $\boldsymbol{R}$ the equilibrium internuclear distance ($|R| = 2$ au for an H_2^+ molecule). Furthermore, $s(R) = \exp(-R)(3 + 3R + R^2)/3$ is the overlap integral between the two atomic orbitals.

For the final electronic state, $\chi_f^-(t)$, we can choose from three different approximations, according to the choice of the distortion potential to be included explicitly in the wave function, namely:

(i) If we neglect the laser field also in the exit-electronic state, i.e. choosing the same electronic Hamiltonian H_0 as in the entrance channel, we arrive at

$$H_f|\chi_f^-\rangle = H_0|\phi_{\boldsymbol{k}}^-\rangle = \epsilon_f|\phi_{\boldsymbol{k}}^-\rangle. \tag{6}$$

Since the solution of one electron in the continuum of a two Coulombian center is not known, we should approximate $\phi_{\boldsymbol{k}}^-$. Several approaches have been used, e.g. to model electron–molecule collisions (see e.g. [10]). For our purpose we approximate the two-center electronic wave function as [11,40]

$$\phi_{\boldsymbol{k}}^{(-),TCC}(\boldsymbol{r}, t) = \exp(-i\epsilon_f t)\frac{\exp(i\boldsymbol{k}\cdot\boldsymbol{r})}{(2\pi)^{3/2}} C(\boldsymbol{k}, \boldsymbol{r}_1)C(\boldsymbol{k}, \boldsymbol{r}_2) \tag{7}$$

with

$$C(\boldsymbol{k}, \boldsymbol{r}_j) = N(\nu)_1F_1[-i\nu, 1, -i(kr_j + \boldsymbol{k}\cdot\boldsymbol{r}_j)], \quad j = 1, 2. \tag{8}$$

Here, $N(\nu) = \exp(\pi\nu/2)\ \Gamma(1 + i\nu)$ is the usual Coulomb normalization factor and $\nu = Z_j/k$, $Z_j = 1$ the charge of each ionic core. Each of these wave functions corresponds to the well-known solution of the two-body Coulomb continuum problem with incoming boundary conditions. Equation (7) is inspired in the Pluvinage-approach for helium-like systems, with one of the nuclei of H_2^+ replacing the second electron in the equation of He (see [8] and references therein).

(ii) If we neglect the Coulomb interactions in the final channel, i.e. we consider the electron moving *freely* in the laser field, it is possible to write

$$i\frac{\partial}{\partial t}|\chi_f^-(t)\rangle = H_f|\chi_f^-(t)\rangle = \left(\frac{p^2}{2} + V_L(t)\right)|\chi_f^-(t)\rangle. \tag{9}$$

The solution of this last equation are the well-known Volkov states [42]:

$$\chi_{\boldsymbol{k}}^{(-),V}(\boldsymbol{r}, t) = \exp(-i\epsilon t)\frac{\exp(i\boldsymbol{k}\cdot\boldsymbol{r})}{(2\pi)^{3/2}}\mathcal{L}_V^-(\boldsymbol{k}, \boldsymbol{r}, \sqcup) \tag{10}$$

with

$$\mathcal{L}_V^-(\boldsymbol{k}, \boldsymbol{r}, t) = \exp\left(i\boldsymbol{A}^-(t)\cdot\boldsymbol{r} - i\boldsymbol{k}\cdot\int_{+\infty}^{t} dt'\boldsymbol{A}^-(t') - \frac{i}{2}\int_{+\infty}^{t} dt'[\boldsymbol{A}^-(t')]^2\right) \tag{11}$$

and $\boldsymbol{A}^{-}(t) = -\int_{+\infty}^{t} \mathrm{d}t' \boldsymbol{E}(t')$. If we insert the Volkov state (10) into (3) we have the so-called SFA [28].

(iii) Combining the exit-channel wave functions (7) and (10) in a product form, we arrive at the so-called Coulomb–Volkov final state [43,44] extended to the H_2^+ case:

$$\chi_{\boldsymbol{k}}^{(-),CV}(\boldsymbol{r}, t) = \phi_{\boldsymbol{k}}^{(-),TCC}(\boldsymbol{r}, t)\mathcal{L}_V^{-}(\boldsymbol{k}, \boldsymbol{r}, t). \qquad (12)$$

Inserting the distorted wave function (12) into the T-matrix Equation (3) we have the CVA extended to the H_2^+ molecule. Looking at the details of the approximations (i) and (ii) we can easily conclude that both are limiting cases of the approximation in (iii), namely: performing the limit of $Z_j \to 0$ in (7) we arrive at the SFA and, on the other hand, taking the limit of $\mathcal{L}_V^{-}(\boldsymbol{k}, \boldsymbol{r}, t) \to 1$, we recover (i). The CVA for atoms was first proposed in [45] based on the original approaches used in atomic collisions [46,47]. The CVA for atoms has been extensively used to study the near-threshold ionization electron distributions and it was shown to be a powerful alternative tool to the TDSE approaches (see e.g. [35] and references therein).

3. Results and discussion

We will analyze the electron momentum distributions of Equation (2) choosing cylindrical coordinates for the laser-ionized electron momentum $\boldsymbol{k}$. The longitudinal component of $\boldsymbol{k}$, i.e. k_z, is directed along the polarization axis z and the transverse component ($k_\rho = (k_x^2 + k_y^2)^{1/2}$) corresponds to a direction perpendicular to the z-axis. These distributions have already shown to be an excellent scenario to analyze and study the relative importance between the electromagnetic and ionic Coulomb fields in atoms [31,35]. Furthermore, these two-dimensional distributions have been measured experimentally for rare gases [29,30]. As we will show next, these 2D plots also configure a valuable tool to disentangle the interference features that appear when we use molecular species as the system under study.

We start by considering the H_2^+ molecule as an hydrogen-like atom with the same ionization potential, i.e. we will deliberately neglect the two center nature of the molecule. To this end, stating that the ionization potential of the H_2^+ molecule is $I_p = 30$ eV (1.1 au), we could model the molecular system as an hydrogen-like atom with an effective charge $Z_{\mathrm{eff}} = 1.48$. In Figure 1 we show a comparison between the predictions of the SFA (Figure 1(*a*)) and the CVA (Figure 1(*b*)) approaches. We use a laser pulse with a peak field $F_0 = 0.163$ au, a central frequency $\omega_0 = 0.55$ au and a total duration $\tau = 68.5$ au (corresponding to six complete optical cycles). In all the studied cases we consider cosine like pulses, i.e. $\phi_{\mathrm{CE}} = 0$ in (1). The Keldysh parameter ($\gamma = (\omega_0/F_0)(2I_p)^{1/2}$) gives $\gamma = 5$, indicating the dominance of the multiphoton process (it is necessary for at least two photons to ionize the H_2^+ molecule with these laser parameters). We have chosen these laser parameters to compare directly our predictions with those that appeared in atoms [31,35]. In this sense, the SFA and CVA reproduce the overall above threshold

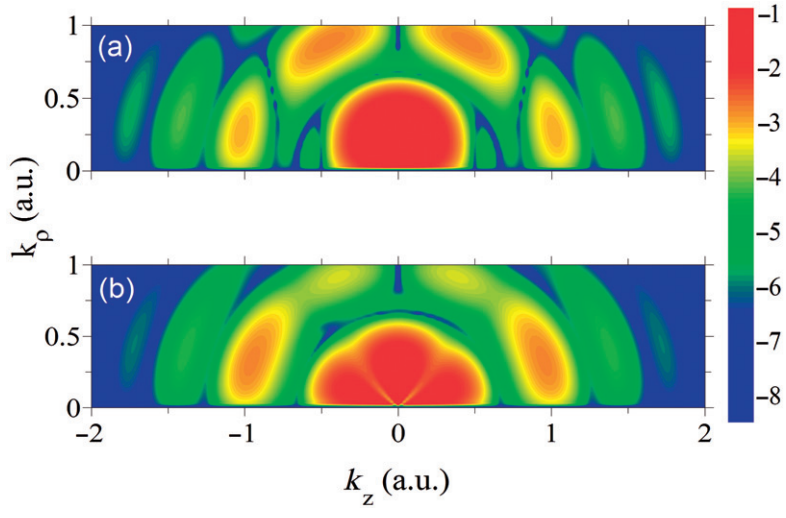

Figure 1. Double-differential electron momentum distributions (logarithmic scale) in cylindrical coordinates (k_z, k_ρ). The parameters of the field are $F_0 = 0.163$ au, $\omega_0 = 0.55$ au and $\tau = 68.5$ au (6 cycles). The H_2^+ molecule is considered as an atom with $I_p = 30$ eV (1.1 au) (see text). The Keldysh parameter is $\gamma = (\omega_0/F_0)(2I_p)^{1/2} = 5$. (*a*) SFA and (*b*) CVA. (The color version of this figure is included in the online version of the journal.)

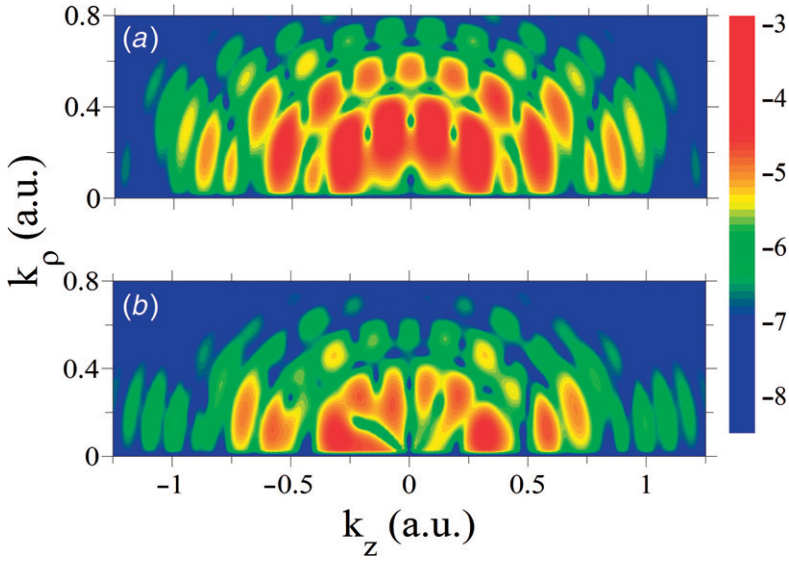

Figure 2. As in Figure 1, but the parameters of the field are now $F_0 = 0.126$ au, $\omega_0 = 0.1125$ au and $\tau = 446.81$ au (8 cycles) ($\gamma = (\omega_0/F_0)(2I_p)^{1/2} = 1.32$). (*a*) SFA and (*b*) CVA. (The color version of this figure is included in the online version of the journal.)

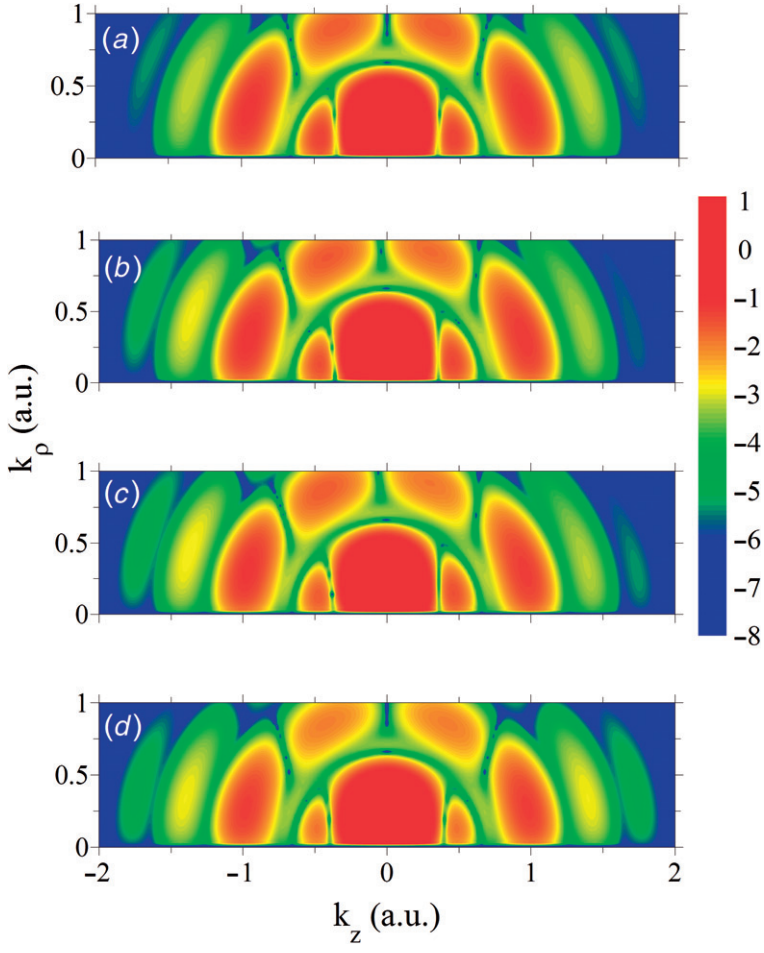

Figure 3. Double differential momentum distributions for the H_2^+ molecule using the two center SFA approach with $|R| = 2$ au. The parameters of the field are as in Figure 1 ($\gamma = 5$). (*a*) 0°, (*b*) 30°, (*c*) 45° and (*d*) 90°. (The color version of this figure is included in the online version of the journal.)

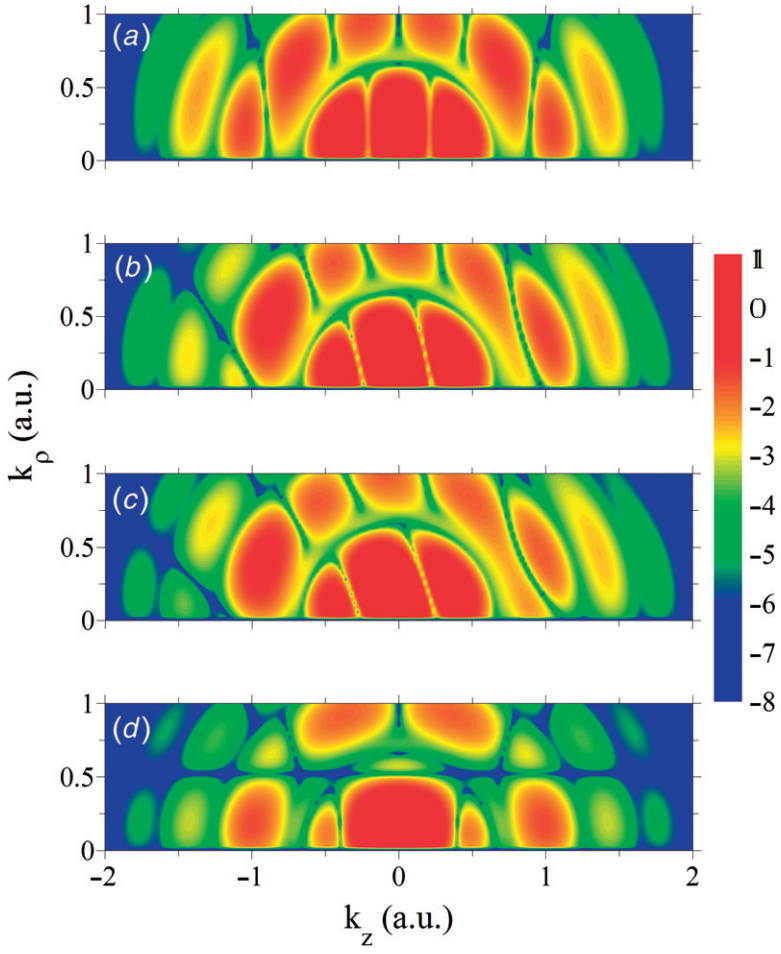

Figure 4. Same as in Figure 3 but for $|R| = 6$ au (*a*) 0°, (*b*) 30°, (*c*) 45° and (*d*) 90°. (The color version of this figure is included in the online version of the journal.)

ionization (ATI) ring pattern that appear in the *ab initio* atomic calculations [31,35]. On the other hand, the near-threshold *bouquet structure* is only reproduced by the CVA. This kind of structure can be attributed to a dominance of a single partial wave [31]. Finally, since these atomic-like models do not depend on the molecular orientation angle, it is not possible to observe differences for different orientation of the H_2^+ molecule with respect to the polarization axis (see above).

Rather than a multiphoton process, laser-ionization is led by barrier tunneling or even above-barrier transitions for smaller Keldysh parameters. In Figure 2 we present comparisons between the SFA (Figure 2(*a*)) and the CVA (Figure 2(*b*)) for an eight-cycle ($\tau = 447$ au) pulse with a peak amplitude for the electric field $F_0 = 0.126$ au and a central frequency $\omega_0 = 0.1125$ au, which corresponds to a Keldysh parameter $\gamma = 1.32$. This value of γ could be considered in the *transition* zone between the multiphoton and tunneling regimes. As in the case of the hydrogen atom analyzed by Arbó et al. [35] the SFA and CVA models are only in quantitative agreement with the exact *ab initio* results. A major difference, however, appears, namely, the intensity of the ATI rings in the approximated models decrease much more rapidly with increasing energy than the TDSE predictions. This can be easily explained since in both approximated models re-scattering events are neglected, meanwhile in the TSDE all the laser-induced mechanisms are included.

Following the arguments pointed out by Arbó et al. [35] we will concentrate our studies in only two Keldysh parameter cases: $\gamma = 5$ and $\gamma = 1.32$. In these two cases we could safely argue that the approximated models, both the SFA and the CVA, and mainly this latter, can be a valuable alternative to the TDSE solution schemes.

Our next step is to introduce in the formalisms the multi-center nature of the H_2^+ molecule and to study their implications. In Figure 3 we show double differential momentum distributions for the H_2^+ molecule illuminated by a laser pulse with the same

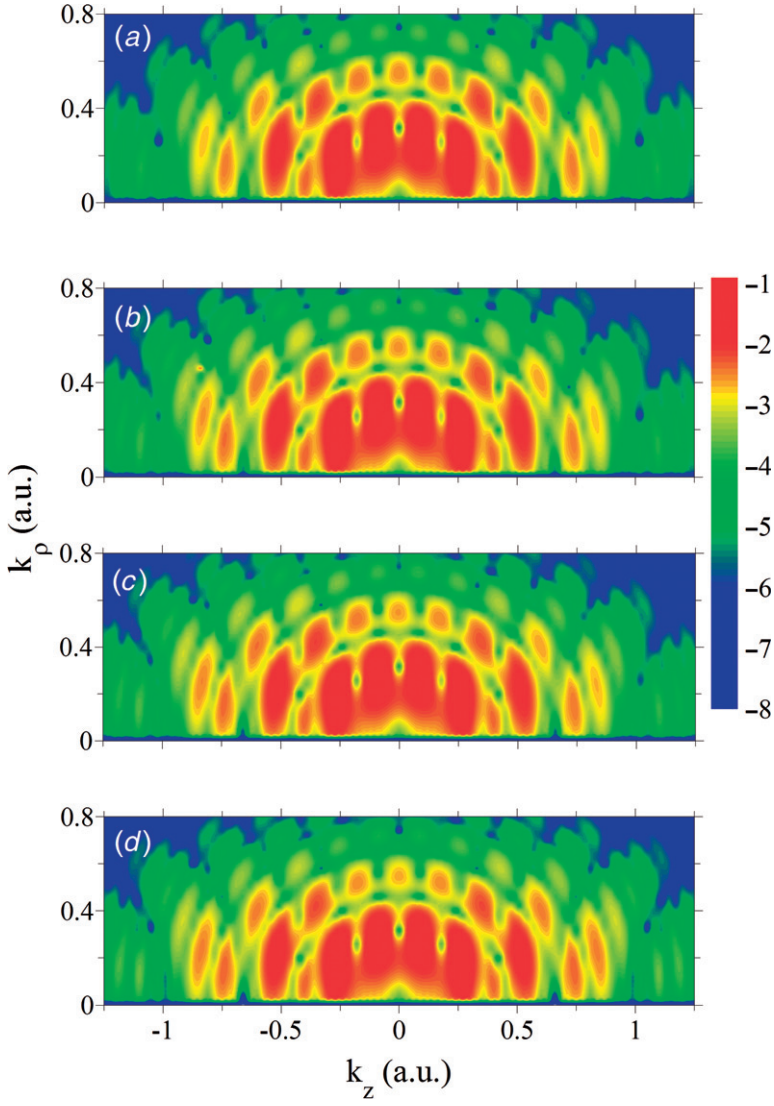

Figure 5. Double differential momentum distributions for the H_2^+ molecule using the two center SFA approach with $|R| = 2$ au. The parameters of the field are as in Figure 2 ($\gamma = 1.32$). (*a*) 0°, (*b*) 30°, (*c*) 45° and (*d*) 90°. (The color version of this figure is included in the online version of the journal.)

parameters as in Figure 1, i.e. $\tau = 68.5$ au, $F_0 = 0.163$ au, $\omega = 0.55$ au and $\gamma = 5$ and using the SFA formalism. For the molecule we have used its *true* parameters: $I_p = 1.1$ au (30 eV) and $|R| = 2$ au. The panels represent different orientations of the molecule with respect to the laser polarization axis (z-axis): (*a*) 0° (parallel to the polarization axis), (*b*) 30°, (*c*) 45° and (*d*) 90° (perpendicular to the polarization axis). Two main important observations can be made (i) the distributions seem to be *insensitive* to the molecular orientation angle and (ii) for electron energies near the threshold *bouquet-type* structures are absent, which is expected since the Coulomb interaction of the ionic cores are neglected in the present SFA formalism. A physical explanation of the former can be traced out in terms of the De Broglie wavelength of the laser-ionized electron (see the discussion below).

In order to enhance the molecular features in the double differential momentum distributions we have deliberately set the intermolecular distance to $|R| = 6$ au. Even when the experimental realization of this situation is unreachable nowadays, this condition could be naturally created by exciting the H_2^+ molecule from its ground state, starting from its equilibrium internuclear distance $|R| = 2$ au, to a dissociative state. Studies of laser–matter processes using *stretched* molecules have been presented already [13,18,48,49]. The double differential electron distributions for this case, using the SFA formalism and the same laser parameters as in Figures 1 and 3, are shown in Figure 4.

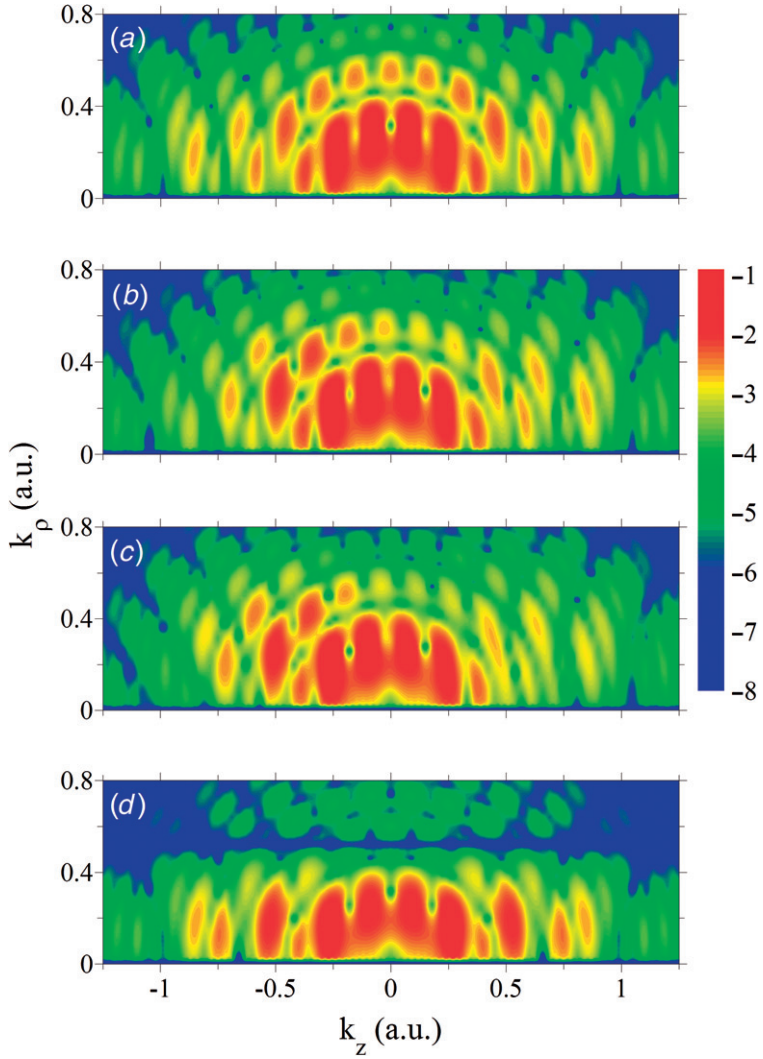

Figure 6. Double differential momentum distributions for the H_2^+ molecule using the two center SFA approach with $|R| = 6$ au. The parameters of the field are as in Figure 2 ($\gamma = 1.32$). (*a*) 0°, (*b*) 30°, (*c*) 45° and (*d*) 90°. (The color version of this figure is included in the online version of the journal.)

The panels represent different orientations of the H_2^+ molecule with respect to the laser polarization axis (z-axis): (*a*) 0° (parallel to the polarization axis), (*b*) 30°, (*c*) 45° and (*d*) 90° (perpendicular to the polarization axis). In these plots it is possible to clearly observe *interference fringes* as a consequence of the presence of two atomic centers, i.e. our *stretched* molecule enhances the interference features. Furthermore, these *fringes* rotate as the orientation of the molecule change, defining a clear *line of minima* for $k_\rho \approx 0.5$ au for the perpendicular orientation case (90°).

For the sake of completeness we have also calculated double differential momentum distributions using the SFA formalism for the case of a Keldysh parameter $\gamma = 1.32$. The results are shown in Figures 5 and 6. Although less pronounced and *mixed* with the electron path interference [35], it is possible to observe interference patterns for $|R| = 6$ au (Figure 6) and such structures are comparable to those shown in Figure 4 since they are independent of the laser parameters (see discussion below).

A deeper study of the combined effects of the two competing fields can be performed applying the CVA model described in (iii) of Section 2. In order to avoid dealing with two center integrals in the numerical calculation of (3), we further approximate the Coulomb continuum wave functions $C(\boldsymbol{k}, \boldsymbol{r}_1)$ and $C(\boldsymbol{k}, \boldsymbol{r}_2)$ of (8) by their zeroth order around each nuclei [50], i.e. $C(\boldsymbol{k}, \boldsymbol{r}_1) \approx C(\boldsymbol{k}, \boldsymbol{R})$ and $C(\boldsymbol{k}, \boldsymbol{r}_2) \approx C(\boldsymbol{k}, -\boldsymbol{R})$, respectively. Using this approximation it is

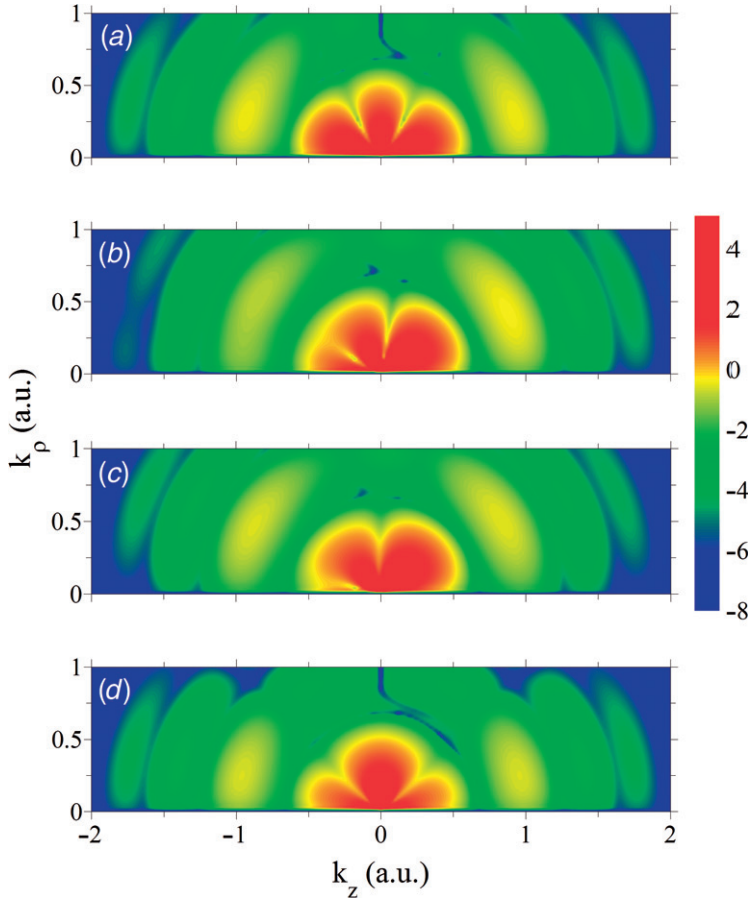

Figure 7. Double differential momentum distributions for the H_2^+ molecule using the two center CVA approach with $|R| = 2$ au. The parameters of the field are as in Figure 1 ($\gamma = 5$). (*a*) 0°, (*b*) 30°, (*c*) 45° and (*d*) 90°. (The color version of this figure is included in the online version of the journal.)

possible to show an improvement in the description of the recombination step in the HHG in H_2^+ molecules [11] that is related with the laser-induced process we are analyzing in this work (see discussion below). In Figure 7 we plot double differential momentum distributions for the H_2^+ molecule using the two center CVA approach. The laser parameters are as in Figure 1, i.e. $\tau = 68.5$ au, $F_0 = 0.163$ au, $\omega = 0.55$ au and $\gamma = 5$. We choose the *real* internuclear distance, i.e. $|R| = 2$ au and the panels represent different molecular orientation angles, namely: (*a*) 0°, (*b*) 30°, (*c*) 45° and (*d*) 90°. Although a clear interference pattern is not visible, we can observe that the *bouquet*-type structure is present and barely changes with the molecular orientation angle.

As we made in the SFA case, here it is also interesting to set the internuclear distance to $|R| = 6$ au. The double differential momentum distributions using this value of $|R|$ are shown in Figure 8. We can see that the structures near the threshold are strongly influenced by the orientation angle and it is possible to observe a clear *curved* line of minima for $\theta = 90°$. This line tends to a straight line whose limit is $k_\rho = 0.5$ au, which corresponds to the predictions of the two-slit formula (see the discussion below).

In order to complete the feasibility of our CVA formalism, we have calculated double differential momentum distributions for the case of a Keldysh parameter $\gamma = 1.32$. The results are shown in Figures 9 and 10. As in the case of Figures 7 and 8, the structures near the threshold are now present and for the case of larger internuclear distance, a clear interference pattern is also visible.

A better analysis of the interference patterns can be performed analyzing double differential momentum distribution (2) as a dipole moment, i.e.

$$\frac{d\widetilde{P}}{d\boldsymbol{k}} \propto \langle \chi_f^- | z | \phi_i \rangle, \tag{13}$$

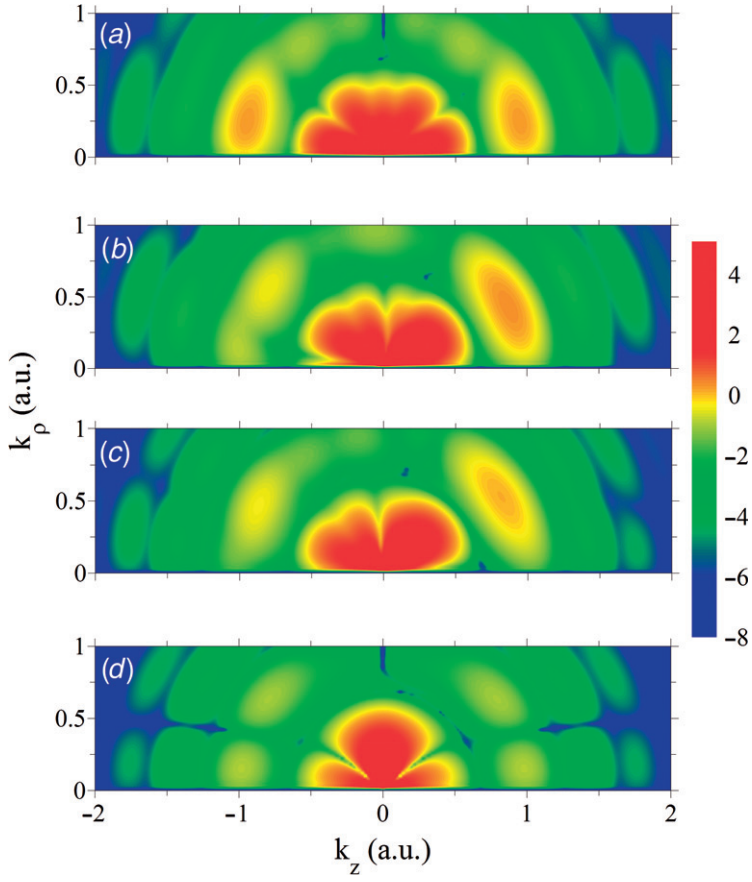

Figure 8. Same as in Figure 7 but for $|R| = 6$ au. (*a*) 0°, (*b*) 30°, (*c*) 45° and (*d*) 90°. (The color version of this figure is included in the online version of the journal.)

since the electric field has only one component along the z-axis and where only the *spatial* part of $\langle\chi_f^-|$ and $|\phi_i\rangle$ is used. In this way, we are able to produce a *clean* picture of the two center interference, since the path electron interferences due to the laser field are absent [31,35]. In Figures 11 and 12 we plot (13) as a function of the (k_z, k_ρ) using the SFA and CVA formalisms. According to the arguments pointed out above, we have performed these graphs using $|R| = 6$ au and for different orientation angles: (*a*) 0° (parallel to the polarization axis), (*b*) 30°, (*c*) 75° and (*d*) 90° (perpendicular to the polarization axis). An interference pattern, which changes as the molecule is rotated in the space, is clearly observable.

We start analyzing a related process in H_2^+ molecules: the HHG. It was demonstrated by Lein et al. [12] that an interference pattern appears in the HHG of H_2^+, when the spectrum of the radiation is considered in the polarization direction. These interference minima are mainly dictated by the recombination step [1], considering the HHG modeled by the three-step or Lewenstein model [28]. The position of these minima in the HHG spectrum changes as the molecule changes its orientation angle. Using a simple argument the minima in the spectra can be predicted considering that the electromagnetic radiation is emitted by the two atomic centers and interfere with each other [13]. Considering the recombination step in the length gauge for H_2^+ [11] and analyzing only recombination along the laser polarization axis [13], we can argue that it has the same functional structure of (13). Additionally, in our laser-induced ionization process the situation is even richer, since we have at our disposal a two electron momentum distribution to study and analyze the interference patterns. It was already shown by Torres [51] that the characteristics of the molecular orbital can leave footprints in the electronic dipole moment, analyzed as *dipole maps*. As was mentioned in this work, the strong-field ionization of molecules presents a promising alternative in order to extract molecular structure due to its simpler implementation from an experimental point of view.

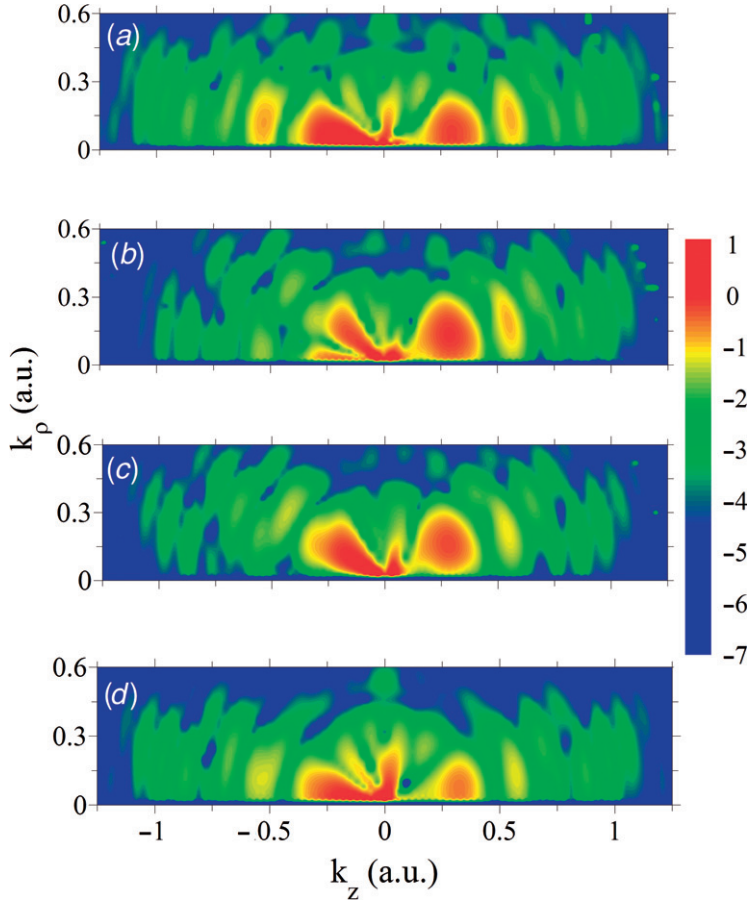

Figure 9. Double differential momentum distributions for the H_2^+ molecule using the two center CVA approach with $|R| = 2$ au. The parameters of the field are as in Figure 2 ($\gamma = 1.32$). (*a*) 0°, (*b*) 30°, (*c*) 45° and (*d*) 90°. (The color version of this figure is included in the online version of the journal.)

By considering that an interference minima should appear when [13]:

$$\boldsymbol{k} \cdot \boldsymbol{R} = (2n+1)\pi, \tag{14}$$

n being an integer, we can write (14), using our cylindrical coordinates (k_z, k_ρ), as:

$$k_z R\cos\theta + k_\rho R\sin\theta = (2n+1)\pi, \tag{15}$$

θ being the angle that the H_2^+ subtends with the polarization angle (z-axis). Replacing in (15) $|R| = 6$ au we have

$$k_z\cos\theta + k_\rho\sin\theta = (2n+1)\frac{\pi}{6}. \tag{16}$$

Consequently, the interference patterns should emerge in the two-dimensional electron distributions as straight lines given by Equation (16). In Figure 11 we have superimposed these straight lines, to the dipole transition matrix distributions (13), for (*a*) 0° (parallel to the polarization axis), (*b*) 30°, (*c*) 75° and (*d*) 90° (perpendicular to the polarization axis). We can observe that the agreement between the predictions of the CVA and (16) is almost perfect when the energy (momentum) of the electron is sufficiently high. The presence of the patterns on this region configure a challenge from an experimental point of view, since the cross-sections associated with these electron energies are very small indeed. Nevertheless, considering an adequate set of laser parameters, a substantial part of the interference picture present in Figure 11 could be observable.

From the interference patterns predicted by the CVA formalism (Figure 11) it would be possible, in principle, to retrieve the intramolecular distance $|R|$, as well as its orientation angle θ. The internuclear distance $|R|$ can be calculated starting from the position of the line of minima as a function of k_z or k_ρ (see Figure 11). As an example, we can extract the position of the k_z when $k_\rho = 4$ au from Figure 11(*a*), i.e. $k_z \approx 0.5$ au. Since this figure corresponds to $\theta = 0°$, we

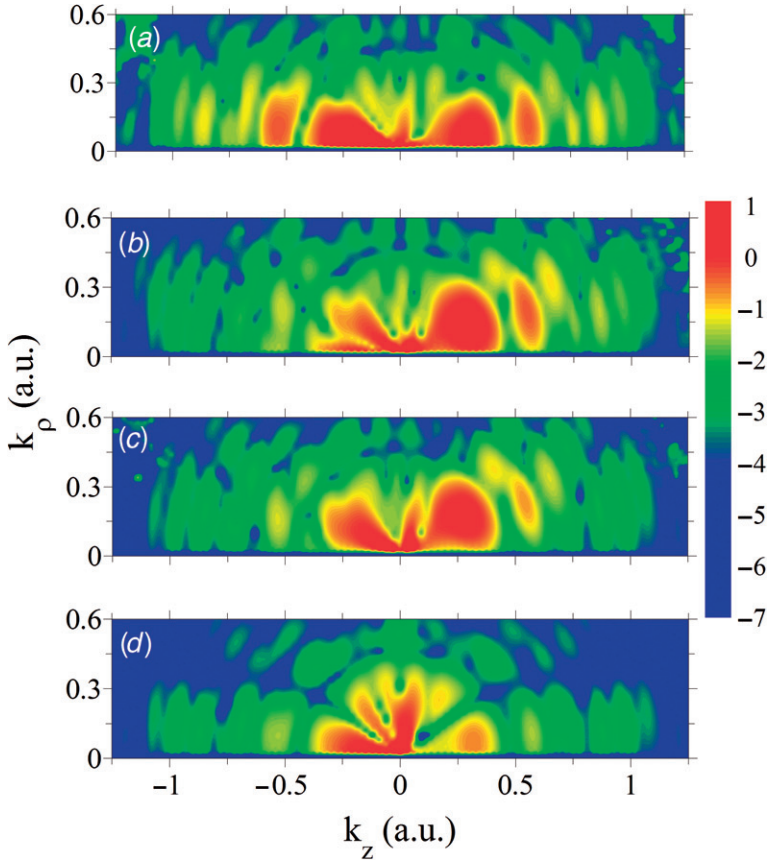

Figure 10. Double differential momentum distributions for the H_2^+ molecule using the two center CVA approach with $|R| = 6$ au. The parameters of the field are as in Figure 2 ($\gamma = 1.32$). (*a*) 0°, (*b*) 30°, (*c*) 45° and (*d*) 90°. (The color version of this figure is included in the online version of the journal.)

can invert (15) setting $n = 0$ and obtain the value of $|R| \approx 6$ au, which corresponds to the value set up in the numerical calculations. The retrieval of the orientation angle is more involved, but can be obtained, however, from Figure 11, as follows. From Figure 11(*a*) we can observe that for $\theta = 0°$ the lines of minima correspond to straight lines parallel to the k_ρ-axis. Consequently, we could argue that the angle between k_z and k_ρ, i.e. the *slope* of the straight lines, form an angle that is complimentary to θ. Consequently, from panels (*b*) or (*c*) of Figure 11 we can easily obtain the value of θ as $\theta = (\pi/2) - \tan^{-1}(k_\rho/k_z)$. Considering the SFA formalism of Figure 12 we can observe that, even when an interference pattern is present, the position of the lines of minima are not at the positions predicted by (16), although the *slope* is the same as in the CVA case.

We can also give physical arguments to explain why near the threshold the interference patterns are absent. When the De Broglie wavelength associated with the laser-ionized electron, i.e. $\lambda = 2\pi/k$ is larger than the distance between the two atomic centers $|R|$, the electron is not able to *resolve* the molecular structure. On the other hand, for a sufficient energetic electron, we have that the electron can serve as a *probe* of the molecular properties. Since, $k^2 = k_z^2 + k_\rho^2$, it is possible to define a circle of constant radius k in the k-plane to approximately separate these two regions. In Figure 13 we can observe how these predictions behave for $|R| = 2$ au and for $|R| = 6$ au.

4. Conclusions and perspectives

We have calculated double-differential electron momentum distributions for laser-induced ionization of H_2^+ molecules using an extension of the CVA for this particular molecular case. To this end we have proposed a model for the final electronic state, in which the laser-ionized electron is influenced by the two remaining atomic cores. On the other hand, we have pointed out the differences of the CVA model with the SFA, in

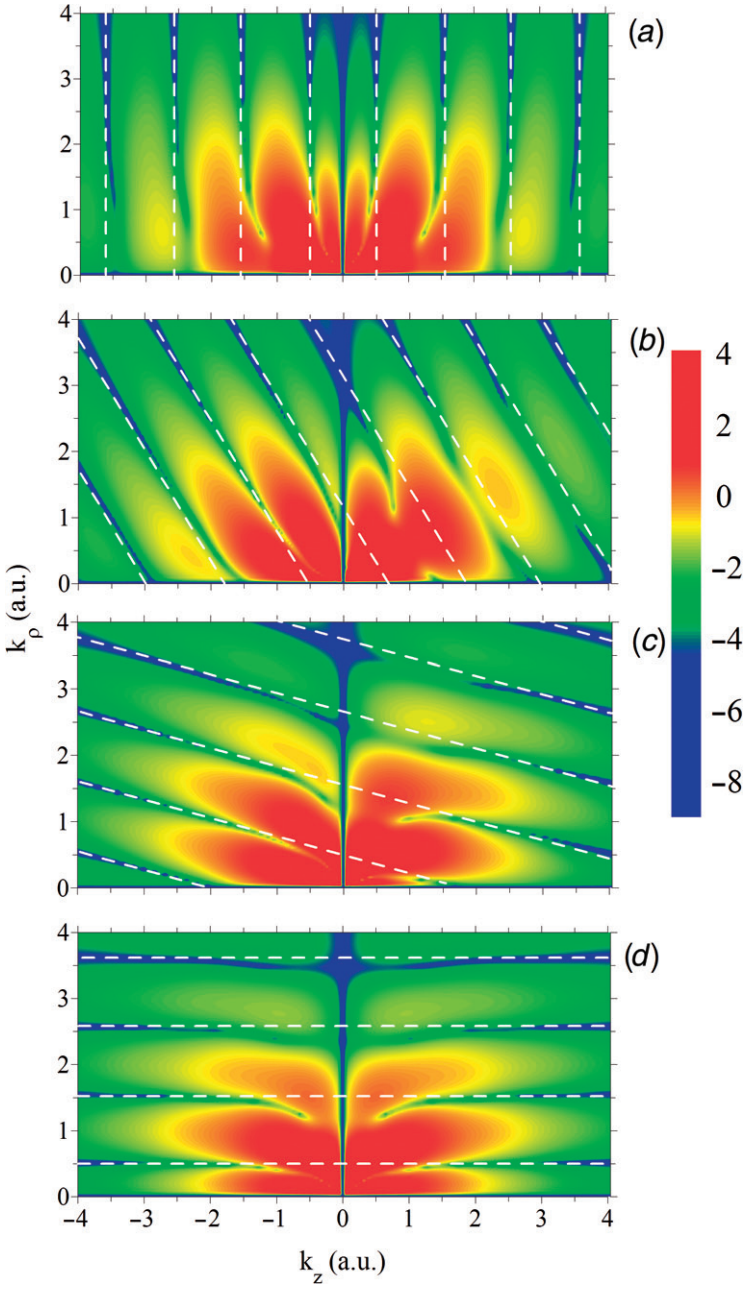

Figure 11. Double differential momentum distributions predicted by the CVA model for the H_2^+ molecule using the *time independent* dipole moment (13) with $|R| = 6$ au (*a*) 0°, (*b*) 30°, (*c*) 75° and (*d*) 90°. The dashed lines correspond to the solution of the two-slit formula (see text). (The color version of this figure is included in the online version of the journal.)

which the Coulomb interaction is completely neglected after the end of the laser pulse.

The results show a concrete influence of the two atomic centers, giving origin to an interference picture. Considering an atomic-like model for the H_2^+ molecule it is possible to observe the absence of this feature, consequently supporting our asseveration that it is intrinsically a characteristic of the molecule. In order to enhance the two center nature of the distributions we have deliberately *stretched* the molecule to emphasize it. In these calculations it is possible to observe how the interference picture varies when the molecule is rotated with respect to the polarization axis of the electromagnetic radiation.

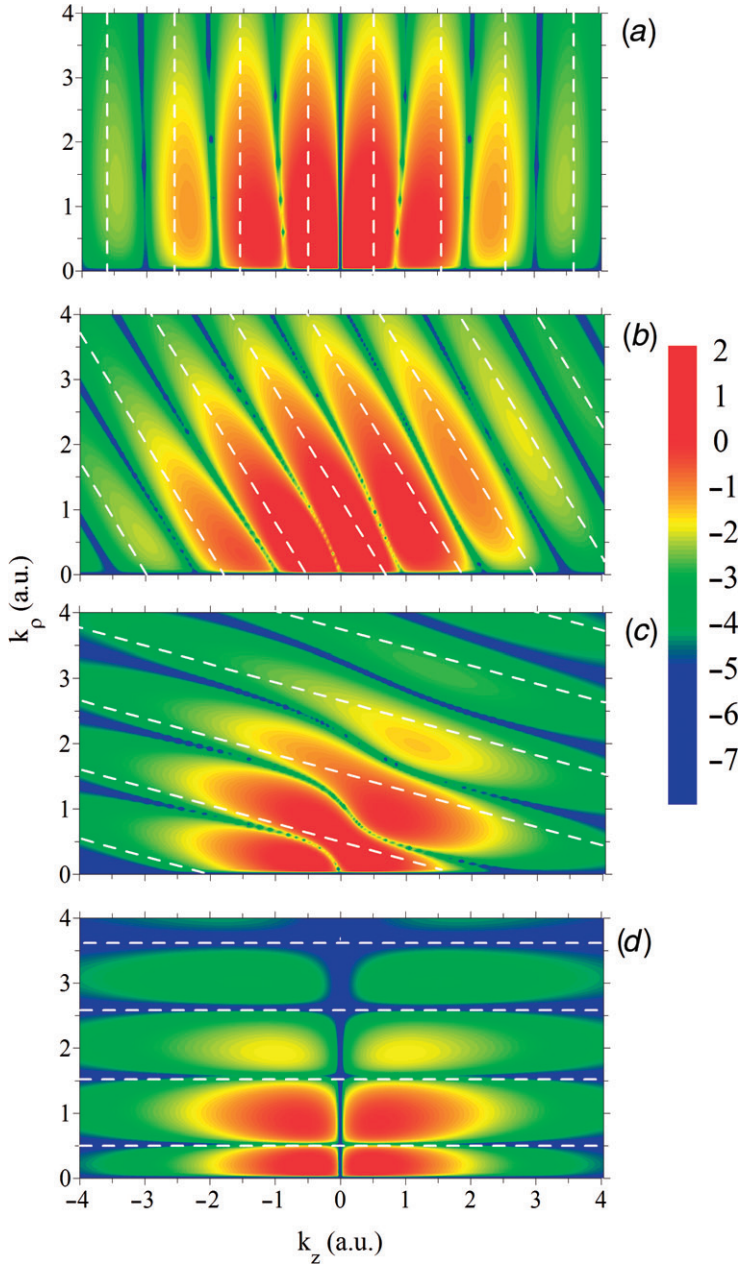

Figure 12. Same as Figure 11 but using the SFA model. (*a*) 0°, (*b*) 30°, (*c*) 75° and (*d*) 90°. The dashed lines correspond to the solution of the two-slit formula (see text). (The color version of this figure is included in the online version of the journal.)

Ultimately, the information present in the double-differential electron momentum distributions could be used to extract information about both the inter-nuclear distance and the orientation angle. As in the case of atoms, a complex structure for electron energies near the threshold is only accounted for when the Coulomb interaction is included in the formalism. Therefore, the present approach has the potential to be a valuable alternative to the *ab initio* methods, as was already demonstrated in the case of atoms. In order to compare theoretical predictions with real experiments, it is commonly argued as a fundamental requisite to perform an average over the laser intensities, where the formalism presented in this work could play an important role, due to its easy and fast numerical implementation.

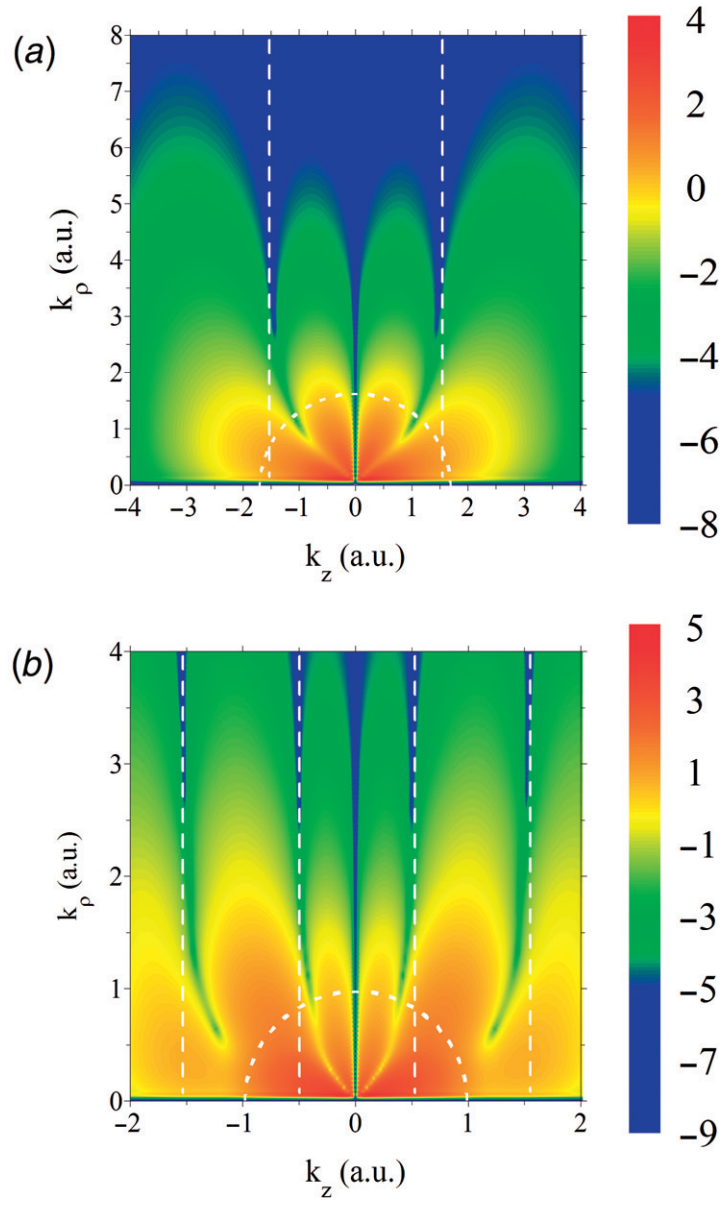

Figure 13. Double differential momentum distributions predicted by the CVA model for the H_2^+ molecule using the *time independent* dipole moment (13). (*a*) $|R| = 2$ au and (*b*) $|R| = 6$ au. The dashed lines correspond to the solution of the two-slit formula and the circles separate the regions where the ionized electron *see* the molecular structure (see text). (The color version of this figure is included in the online version of the journal.)

Acknowledgments

This work was partially supported by ANPCyT under PICTO UNS 931. MFC acknowledges the Visitors Program of the Max Planck Institute for the Physics of Complex Systems for financial support. Useful discussions with D. Arbó and C. Chirilă are gratefully acknowledged.

References

[1] Lein, M. *J. Phys. B* **2007,** *40,* R135–R173.

[2] Martín, F.; Fernández, J.; Havermeier, T.; Foucar, L.; Weber, Th.; Kreidi, K.; Schöffler, M.; Schmidt, L.; Jahnke, T.; Jagutzki, O.; Czasch, A.; Benis, E.P.; Osipov, T.; Landers, A.L.; Belkacem, A.; Prior, M.H.; Schmidt-Böcking, H.; Cocke, C.L.; Dörner, R. *Science* **2007,** *315,* 629–633.

[3] Fernández, J.; Fojón, O.; Palacios, A.; Martín, F. *Phys. Rev. Lett.* **2007,** *98,* 043005.

[4] Stia, C.R.; Fojón, O.A.; Weck, P.F.; Hanssen, J.; Rivarola, R.D. *J. Phys. B* **2003,** *36,* L257–L264.

[5] Kamalou, O.; Chesnel, J.Y.; Martina, D.; Hanssen, J.; Stia, C.R.; Fojón, O.A.; Rivarola, R.D.; Frémont, F. *Phys. Rev. A* **2005,** *71,* 010702(R)-1–4.

[6] Stolterfoht, N.; Sulik, B.; Hoffmann, V.; Skogvall, B.; Chesnel, J.Y.; Rangama, J.; Frémont, F.; Hennecart, D; Cassimi, A.; Husson, X.; Landers, A.L.; Tanis, J.A.; Galassi, M.E.; Rivarola, R.D. *Phys. Rev. Lett.* **2001,** *87,* 023201-1–4.

[7] Ciappina, M.F.; Rivarola, R.D. *J. Phys. B* **2008,** *41,* 015203-1–7.

[8] Juolakian, B.E.; Hanssen, J.; Rivarola, R.D.; Motassim, A. *Phys. Rev. A* **1996,** *54,* 1473–1479.

[9] Weck, P.F.; Fojón, O.A.; Juolakian, B.E.; Stia, C.R.; Hanssen, J.; Rivarola, R.D. *Phys. Rev. A* **2002,** *66,* 012711-1–8.

[10] Galassi, M.E.; Rivarola, R.D. *Phys. Rev. A* **2004,** *70,* 032701-1–13.

[11] Ciappina, M.F.; Chirilă, C.C.; Lein, M. *Phys. Rev. A* **2007,** *75,* 043405-1–7.

[12] Lein, M.; Hay, H.; Velotta, R.; Marangos, J.P.; Knight, P.L. *Phys. Rev. Lett.* **2002,** *88,* 183903-1–4.

[13] Lein, M.; Hay, H.; Velotta, R.; Marangos, J.P.; Knight, P.L. *Phys. Rev. A* **2002,** *66,* 023805-1–6.

[14] Lein, M.; Marangos, J.P.; Knight, P.L. *Phys. Rev. A* **2002,** *66,* 051404-1–4.

[15] Lein, M.; Corso, P.P.; Marangos, J.P.; Knight, P.L. *Phys. Rev. A* **2003,** *67,* 023819-1–6.

[16] Lagmago Kamta, G.; Bandrauk, A.D. *Phys. Rev. A* **2004,** *70,* 011404-1–4.

[17] Lagmago Kamta, G.; Bandrauk, A.D. *Phys. Rev. A* **2005,** *71,* 053407-1–19.

[18] Hetzheim, H.; Figueira de Morisson Faria, C.; Becker, W. *Phys. Rev. A* **2007,** *76,* 023418-1–9.

[19] Gonoskov, A.A.; Gonoskov, I.A.; Ryabikin, M.Yu.; Sergeev, A.M. *Phys. Rev. A* **2008,** *77,* 033424-1–7.

[20] Burnett, K.; Reed, V.C.; Cooper, J.; Knight, P.L. *Phys. Rev. A* **1992,** *45,* 3347–3349.

[21] Dionissopoulou, S.; Mercouris, T.; Lyras, A.; Nicolaides, C.A. *Phys. Rev. A* **1997,** *55,* 4397–4406.

[22] Delone, N.B.; Krainov, V.P. *J. Opt. Soc. Am. B* **1991,** *8,* 1207–1211.

[23] Miloševic, D.B.; Paulus, G.G.; Becker, W. *Opt. Express* **2003,** *11,* 1418–1429.

[24] Macri, P.A.; Miraglia, J.E.; Gravielle, M.S. *J. Opt. Soc. Am. B* **2003,** *20,* 1801–1806.

[25] Rodríguez, V.D.; Cormier, E.; Gayet, R. *Phys. Rev. A* **2004,** *69,* 053402-1–8.

[26] Faisal, F.H.M.; Schlegel, J. *J. Phys. B* **2005,** *38,* L223–L231.

[27] Lewenstein, M.; Kulander, K.C.; Schafer, K.J.; Bucksbaum, P.H. *Phys. Rev. A* **1995,** *51,* 1495–1507.

[28] Lewenstein, M.; Balcou, Ph.; Ivanov, M.; L'Huillier, A.; Corkum, P.B. *Phys. Rev. A* **1994,** *49,* 2117–2132.

[29] Rudenko, A.; Zrost, K.; Schröter, C.D.; de Jesus, V.L.B; Feuerstein, B.; Moshammer, R.; Ullrich, J. *J. Phys. B* **2004,** *37,* L407–L413.

[30] Maharjan, C.M.; Alnaser, A.S.; Litvinyuk, I.; Ranitovic, P.; Cocke, C.L. *J. Phys. B* **2006,** *39,* 1955–1964.

[31] Arbó, D.; Yoshida, S.; Persson, E.; Dimitriou, K.I.; Burgdörfer, J. *Phys. Rev. Lett.* **2006,** *96,* 143003.

[32] Weber, Th.; Weckenbrock, M.; Staudte, A.; Spielberger, L.; Jagutzki, O.; Mergel, V.; Afaneh, F.; Urbasch, G.; Vollmer, M.; Giessen, H.; Dörner, R. *Phys. Rev. Lett* **2000,** *84,* 443–446.

[33] Moshammer, R.; Feuerstein, B.; Schmitt, W.; Dorn, A.; Schröter, C.D.; Ullrich, J.; Rottke, H.; Trump, C.; Wittmann, M.; Korn, G.; Hoffmann, K.; Sandner, W. *Phys. Rev. Lett.* **2000,** *84,* 447–450.

[34] Dimitriou, K.I.; Arbó, D.G.; Yoshida, S.; Persson, E.; Burgdörfer, J. *Phys. Rev. A* **2004,** *70,* 061401-1–4.

[35] Arbó, D.; Miraglia, J.E.; Gravielle, M.S.; Schiessl, K.; Persson, E.; Burgdörfer, J. *Phys. Rev. A* **2008,** *77,* 013401-1–8.

[36] Rudenko, A; Zrost, K.; Ergler, Th.; Voitkiv, A.B.; Najjari, B; de Jesus, V.L.B.; Feuerstein, B.; Schröter, C.D.; Moshammer, R.; Ullrich, J. *J. Phys. B* **2005,** *38,* L191–L198.

[37] Zhang, T.; Nakajima, T. *Phys. Rev. A* **2007,** *75,* 043403-1–10.

[38] Yudin, G.L.; Patchkovskii, S.; Bandrauk, A.D. *J. Phys. B* **2006,** *39,* 1537–1546.

[39] Yudin, G.L.; Patchkovskii, S.; Corkum, P.B.; Bandrauk, A.D. *J. Phys. B* **2007,** *40,* F93–F103.

[40] Yudin, G.L.; Patchkovskii, S.; Bandrauk, A.D. *J. Phys. B* **2008,** *41,* 045602-1–9.

[41] Dewangan, D.P.; Eichler, J. *Phys. Rep.* **1994,** *247,* 59–219.

[42] Wolkov, D.M. *Z. Phys.* **1935,** *94,* 250–260.

[43] Duchateau, G.; Cormier, E.; Gayet, R. *Eur. Phys. J. D* **2000,** *11,* 191–196.

[44] Duchateau, G.; Cormier, E.; Bachau, H.; Gayet, R. *Phys. Rev. A* **2001,** *63,* 053411-1–11.

[45] Jain, M.; Tzoar, N. *Phys. Rev. A* **1978,** *18,* 538–545.

[46] Cheshire, I. *Proc. Phys. Soc.* **1964,** *84,* 89–98.

[47] Vainstein, L.; Presnyakov, L.; Sobelman, I. *Sov. Phys. JETP* **1964,** *18,* 1383–1387.

[48] Figueira de Morisson Faria, C. *Phys. Rev. A* **2007,** *76,* 043407-1–12.

[49] Rivière, P.; Ruiz, C.; Rost, J.M. *Phys. Rev. A* **2008,** *78,* 033421-1–8.

[50] Yudin, G.L.; Chelkowski, S.; Bandrauk, A.D. *J. Phys. B* **2006,** *39,* L17–L24.

[51] Torres, R.; Marangos, J.P. *J. Mod. Opt.* **2007,** *54,* 1883–1899.